Effect of Arm Length on the Aggregation Structure of Fullerene-Based Star Ionomers

T.-L. Lin,[†] U. Jeng,*[,‡] C.-S. Tsao,[§] W.-J. Liu,[#] T. Canteenwala,[¶] and L. Y. Chiang[¶]

Department of Engineering and System Science, National Tsing Hua University, Hsinchu 300, Taiwan, National Synchrotron Radiation Research Center, Hsinchu 30077, Taiwan, Division of Nuclear Fuel and Material, Institute of Nuclear Energy Research, Lungtan 325, Taiwan, Electronics Research and Service Organization, Industrial Technology Research Institute, Chutung, Hsinchu, 310, Taiwan, and Center for Condensed Matter Sciences, National Taiwan University, Taipei 10617, Taiwan

Received: April 15, 2004; In Final Form: July 18, 2004

Using small angle neutron scattering (SANS) and small-angle X-ray scattering (SAXS), we have studied aqueous solutions of a fullerene-based star ionomer−hexa(sulfobutoxypentylcarboxy)[60]fullerene ($FC_{10}S$). With six sulfobutoxypentyl arms randomly bounded on the C_{60} cage, $FC_{10}S$ demonstrates a good solubility in water. The scattering results show that the water-soluble fullerene-based ionomers of a starlike molecular morphology form rodlike aggregates in water solutions. With the contrast provided by SAXS and SANS, we extract detailed structural information for the rodlike aggregates, including arm distribution, aggregation number ~ 32, and the rod radius and length of 21 Å and 160 Å, respectively. We also extract an averaged ionization factor of ~ 0.03 for the $FC_{10}S$ aggregates, using the structural factor derived from the mean spherical approximation model for the charge interacting aggregates. The aggregation structure changes little within the concentration range studied (0.5−4%). Compared to the aggregation characteristics of FC_4S, a similar fullerene-based ionomer with six shorter sulfobutyl arms, $FC_{10}S$, has a much higher aggregation tendency due to the longer sulfobutoxypentyl arms anchored on the C_{60} cage.

1. Introduction

Water-soluble C_{60}-derivatives are generally believed to be better candidates than C_{60} for practical bio-medical applications due to the significant chemical reactivity retained after the chemical modification of C_{60} for higher water solubility. Up to now, many different types of water soluble C_{60}-deriatives have been reported to have effects in reducing or preventing cells from being attacked by reactive oxygen species.[1] Recently, we have synthesized several fullerene-based derivatives, including $C_{60}(OH)_{18}$ and $C_{60}[(CH_2)_4SO_3Na]_6$ (FC_4S), for potential bio-medical applications in, for instances, free radical scavenging and antioxidant-action facilitating.[2,3] Previous studies showed that the radical scavenging efficiency for the fullerene derivatives relates to their aggregation behaviors in water solutions.[4] We found that FC_4S ionomers form stable globular aggregates of a radius of gyration $R_g \approx 19$ Å in a wide concentration range in water solutions, whereas $C_{60}(OH)_{18}$ forms fractal-like aggregates that grow with increasing concentration. The differences in the aggregation behavior observed partially explained the characteristics of the concentration-dependent free radical scavenging efficiency measured for the fullerene-derivatives.[4]

Here, we study a modified fullerene-based ionomer $C_{60}[CO(CH_2)_5O(CH_2)_4SO_3Na]_6$ ($FC_{10}S$), with six sulfobutoxypentyl arms extending out from the C_{60} cage nearly two times more than that for FC_4S. We are interested in the aggregation behavior of the fullerene-based ionomers changed by the extended arm length, and the subsequent change in the radical scavenging efficiency. With longer arms anchored on the C_{60} cages, $FC_{10}S$ star ionomers have larger hydrophobic interactions between arms. In addition, the larger mutual penetration of $FC_{10}S$ arms may also facilitate the interactions between the ionized SO_3^- groups of the arms with the high-charge-affinity C_{60} cages of neighboring $FC_{10}S$.

Using SAXS and SANS as a contrast we intend to extract the structural information of $FC_{10}S$ aggregates in aqueous solutions, including the size, the shape, and the aggregation number.[5,6] SAXS is especially sensitive to the C_{60} cages of $FC_{10}S$ aggregates due to the much higher scattering-length−density (SLD $= 19.5 \times 10^{-6}$Å^2) of C_{60}, than that for the aliphatic arms of $FC_{10}S$ (SLD $= 10.4 \times 10^{-6}$Å^2) and water (SLD $= 9.4 \times 10^{-6}$Å^2). Whereas SANS is more sensitive to the arm distribution of $FC_{10}S$ aggregates in D_2O solutions, since the arms of a low SLD, 0.1×10^{-6}Å^2 can be contrasted out by the high SLD of D_2O (6.33×10^{-6}Å^2) and C_{60} cages (7.3×10^{-6}Å^2). In small angle scattering (SAS), form factors of ionomer aggregates usually convolute significantly with structure factors due to the prominent interference caused by charge interactions. To extract the aggregation structure and charge interaction characteristics of the fullerene-based ionomers from the contrast SAS data, we adopt a model consisting of rodlike form factor and a structural factor of charge-interacting characteristics in a model-fitting algorithm, as detailed in the followings.

2. Scattering Model

Small angle scattering profiles for colloidal aggregates of a monodisperse size can be modeled as[7]

$$I(Q) = I_o \tilde{P}(Q) S(Q) \tag{1}$$

* To whom correspondence should be addressed. Fax: 886−3−5780281, ext.7108; E-mail: usjeng@nsrrc.org.tw.
[†] National Tsing Hua University.
[‡] National Synchrotron Radiation Research Center.
[§] Institute of Nuclear Energy Research.
[#] Industrial Technology Research Institute.
[¶] National Taiwan University.

10.1021/jp048335g CCC: $27.50
Published on Web 08/31/2004

where $\tilde{P}(Q)$ is the normalized form factor with $\tilde{P}(0) = 1$, and $S(Q)$ is the structure factor with $S(Q) \sim 1$ at large Q values. The wave vector transfer $Q = 4\pi\sin(\theta/2)/\lambda$ is defined by the scattering angle θ and wavelength λ of X-rays or neutrons. Also, $I_o = CN(b - \rho_w V)^2$ is the scattering amplitude with the concentration C, the aggregation number N, and the dry volume V for the scattering particles. The scattering length for the particles and scattering-length density for the solvent are denoted by b and ρ_w, respectively. For homogeneous rodlike particles of radius R and length L, the spatial-orientation averaged form factor is

$$\tilde{P}(Q) = \int_0^1 \left|\frac{2J_1(v)}{v}\frac{\sin(w)}{w}\right|^2 d\mu \qquad (2)$$

with $v = QR(1 - \mu^2)^{1/2}$, $w = (1/2)QL\mu$, and the first-order Bessel function J_1.[8,9] Neglecting the structural factor in the intermediate Q range where $S(Q) \sim 1$, $QL < 1$, and $QR_c < 1$ (Kratky-Porod approximation),[10] we can approximate the scattering intensity in (1) and (2) for the rodlike aggregates by

$$QI(Q) = C\pi\frac{N}{L}[b - \rho_w V]^2 \, e^{-1/2Q2R_c^2} \qquad (3)$$

where the radius of gyration for the cross-section of the cylinders, $R_c = R/\sqrt{2}$. With (3), the rod radius R can be extracted conveniently from the slope ($= R_c^2/2$) through the linear relationship of $\ln(QI(Q))$ and Q^2.

For macroion solutions, the structure factor $S(Q)$ depends on the volume fraction η and the fractional ionization α of the aggregates.[11] We adopt the commonly used mean spherical approximation (MSA) and the subroutine originated by Hayter et al.[12] for $S(Q)$ in our study. The MSA model, detailed in many articles,[11,12] assumes rigid charged spheres of a diameter σ interacting with each other through a screened Coulomb potential of a Yukawa form, determined by σ and α (or the net charge) of the aggregates and the dielectric constant ϵ of the solution. For rodlike charge particles, we use $\eta = n_p(\pi R^2 L)$ and an effective hard sphere diameter $\sigma = (6LR^2)^{1/3}$ in the MSA model on a basis of equivalent volume.[11] When the axial ratio $L/2R$ of the rods is larger than 2, a hydrodynamic radius R_h calculated from the rod length and radius is used for the effective diameter ($\sigma = 2R_h$).[13] We, further, correct the $S(Q)$ calculated from the MSA approximation for a nonspherical particle effect (or orientation effect), which is nontrivial for rodlike particles of large axial ratios.[11]

3. Samples and Experiment

The detailed synthesis route for Hexa(sulfobutoxypentylcarboxy)[60]fullerene, $C_{60}[CO(CH_2)_5O(CH_2)_4SO_3Na]_6$ ($FC_{10}S$), was reported previously.[14] SANS measurements for D_2O solutions of 0.5, 1, 2, and 4 wt. % $FC_{10}S$, at 25 °C, were conducted using the eight-meter SANS instrument at the National Institute of Standards and Technology (NIST). Despite the good solubility of the fullerene derivative in water, $FC_{10}S$ shows a sign of sedimentation when the concentration exceeds $\sim$ 4%. On the other hand, the solution of the lowest concentration of 0.5% $FC_{10}S$ gives a marginal SANS intensity for the measurement. The neutron beam, monochromated by a velocity selector with a wavelength dispersion $(\Delta\lambda/\lambda)_{fwhm}$ of 25%, was collimated by two pinholes, with diameters of 2.5 and 1 cm, separated by 4.1 m. With two wavelengths of 5 Å and 12 Å, and a sample-to-detector distance of 3.6 m, the measured SANS data covered a Q range from 0.007 $Å^{-1}$ to 0.2 $Å^{-1}$. The data collected by the two-dimensional detector were corrected for sample transmission, background, and detector sensitivity, and normalized to the scattering cross section per unit sample volume (the absolute intensity).[15] On the other hand, SAXS measurements for the same sample solutions were performed at 25 °C on the 8-m SAXS instrument at the Tsing-Hua University, Hsinchu, Taiwan.[16] The beam, emitted from the 18-kW rotating-anode (copper target), was monochromated by a pyrolytic graphite to a wavelength of 1.54 Å and collimated by three pinholes into a 1.5-mm diameter beam. With two sample-to-detector distances of 4.1 and 2.3 m, the SAXS data covered a Q range from 0.01 to 0.25 $Å^{-1}$. All of the data were collected by a two-dimensional area detector and were normalized to the absolute intensity using the same procedure as that applied for the SANS data.

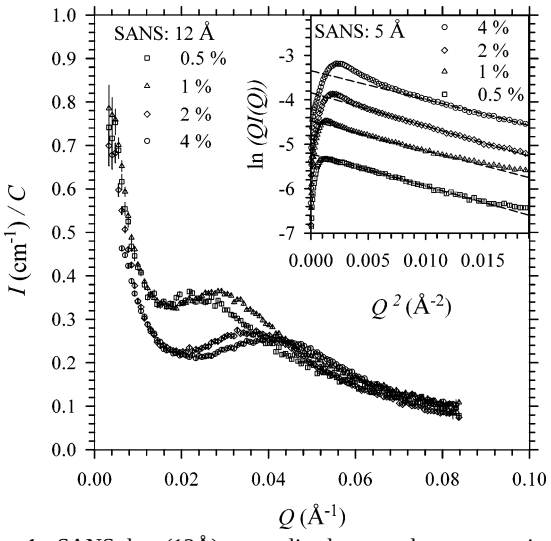

Figure 1. SANS data (12Å), normalized to sample concentration, for the D_2O solutions of 0.5, 1, 2, and 4% $FC_{10}S$. Inset shows the corresponding SANS data (measured with 5 Å) fitted with the Kratky-Porod approximation (dotted curves) for the rodlike characteristics of the aggregates.

4. SAS Results

SANS Data. After being normalized by the concentration, the SANS data measured using 12-Å neutrons for the sample solutions of 0.5, 1, 2, and 4 wt. % of $FC_{10}S$ (Figure 1) overlap well in the higher-Q region ($Q \gtrsim 0.07Å^{-1}$). Further, the four sets of SANS data measured at 5 Å (inset of Figure 1) for the same solutions, for extending data in the Q-region, show rodlike characteristics of similar rod radii for the $FC_{10}S$ aggregates in the concentration range studied.[17] From the slopes of the Kratky−Porod approximation (dotted lines in the inset of Figure 1), similar radii around 17 ± 1 Å for the $FC_{10}S$ rodlike aggregates can be extracted. We have also tried to fit the data to $I(q) \propto \exp(-q^2R_t^2)/q^2$ for a disklike structure, the power law scattering $I(q) \propto q^{-\alpha}$ for a fractal-like structure, or a spherical particle form factor,[8,11] but the results are not as good as that given by the rodlike structure. Furthermore, a model independent method mentioned below also prefers the rodlike shape for the aggregates.

In the lower Q-region, the scattering shoulders of these SANS profiles shift gradually from $Q \sim 0.02$ $Å^{-1}$ for the 0.5% data toward a larger Q value as concentration increases, revealing an increasing interparticle interaction effect, as that commonly seen in many macroion solutions of charge interactions between aggregates.[11] For the even lower Q region ($\lesssim 0.01Å$), all four sets of data merge together and manifest a power-law scattering characteristic of $I(Q) \propto Q^{-4}$, which is likely due to large aggregates in the solutions.[18,19]

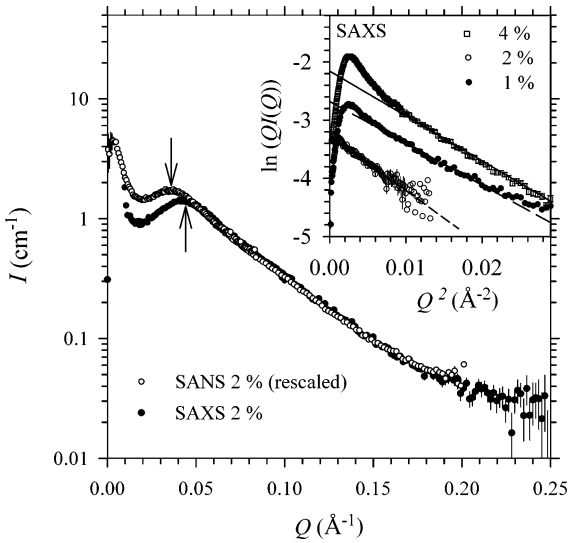

Figure 2. Comparison of the SAXS data with the rescaled (3.2 times) SANS data for the D_2O solution of 2% $FC_{10}S$. The arrows indicate the scattering peaks for the SANS and SAXS profiles, respectively. In the inset, the SAXS data for the 1, 2, and 4% sample solutions are fitted by the Kratky-Porod approximation (dashed curves) of rodlike characteristic features.

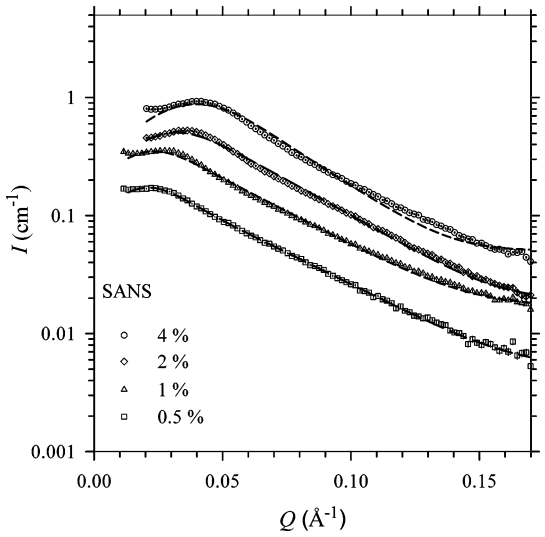

Figure 3. Model-fitting result (dashed curves) for the SANS data of 4%, 2%, 1%, and 0.5% $FC_{10}S$ in water solutions, using a rodlike form factor together with the MSA structural factor.

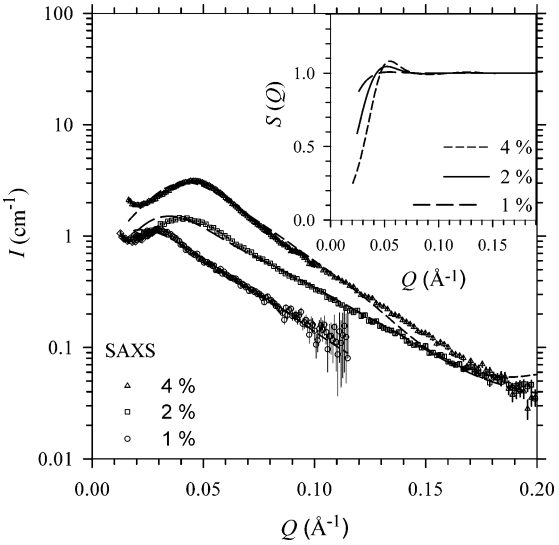

Figure 4. Model-fitting result (dashed curves) for the SAXS data of 4%, 2%, and 1% $FC_{10}S$ in water solutions. The inset shows the corresponding $S(Q)$ calculated from the MSA model.

SAXS Data. The SAXS profiles measured for the D_2O solutions of 1%, 2%, and 4% $FC_{10}S$ are similar to the SANS result. We compare the SAS data for the 2% sample solution in Figure 2. After being scaled up by a factor of 3.2, the SANS profile can overlap the SAXS profile well into the higher Q region ($Q \gtrsim 0.04$ Å^{-1}), revealing the common rodlike feathers. Since neutrons and X-rays are sensitive to the arms and C_{60} cages of $FC_{10}S$, respectively, the similar rod radius of the aggregates of $FC_{10}S$ observed by SANS and SAXS implies a relatively uniform distribution of arms and C_{60} cores in the cross-section direction of the rodlike aggregates. However, the SAXS profile deviates from the SANS profile when Q is smaller than the interference peak at ~ 0.04Å^{-1}. Since the physical aggregation structure and interaction characteristics ($S(Q)$) should be the same for the same solution (2 wt. % for this case), regardless of SANS and SAXS, this deviation in SAS profiles is most likely caused by a structural inhomogeneity in the longitudinal direction of the rodlike aggregates, as we have shown previously that the cross-section of the rodlike aggregates of $FC_{10}S$ are relatively homogeneous. More specifically, the early upturn for the SANS data, namely, a larger $P(Q)$ for SANS, may indicate that the sulfobutoxypentyl arms of $FC_{10}S$ stretch out at both ends of the aggregates and leave the C_{60} cages in an inner region (smaller $P(Q)$ for SAXS) of the cylinder-like aggregates. A structural picture for the aggregates will be given below.

We extract the radius of the rodlike aggregates from the SAXS data using the Kratky−Porod approximation (dashed lines in the inset of Figure 2). The radii, $R = 17.3 \pm 0.5$ Å for the 2% and 4% data, and 19.5 ± 1 Å for the 1% data are similar to those observed in SANS. Furthermore, from the intensity ratio r of the SANS and SANS profiles for the 2% solution (in the Q-region where two profiles overlap), we can also calculate a dry volume V for $FC_{10}S$ using (3), since

$$r = (QI_x)/(QI_n) = [(b_x - \rho_{wx}V)/(b_n - \rho_{wn}V)]^2 \qquad (4)$$

With QI_x and QI_n values at $Q \sim 0$ extrapolated from the Kratky−Porod approximation for the corresponding SAXS and SANS data (see the insets of Figure 1 and Figure 2), we obtain $r = 3.2$. On the other hand, the scattering lengths of $FC_{10}S$ calculated from the molecular formula are $b_x = 3.47 \times 10^{-2}$ Å and $b_n = 6.07 \times 10^{-3}$ Å, and the scattering-length density of water are $\rho_{wx} = 9.4 \times 10^{-6}$ Å^{-2} and $\rho_{wn} = 6.36 \times 10^{-6}$ Å^{-2} (D_2O), for X-rays and neutrons, respectively. Substituting these values into eq 4, we obtain a dry volume $V = 2200$ Å^3 for $FC_{10}S$, which is consistent with an estimated value of 2370 Å^3 using 525, 27, and 80 Å^3 for the dry volumes of C_{60}, CH_2, and SO_3Na, respectively.[20] With the above numerical values, we can also obtain a linear packing density N/L of 0.20 for the rodlike aggregates from eq 3. Similar V and N/L values can be extracted from the 4% and 1% contrast SANS and SAXS data as well.

Model Fitting. Using the structural features observed previously in eq 1, we fit the SAS data measured for the $FC_{10}S$ solutions with a rodlike form factor and a structural factor from the MSA model. The fitting parameters are (a) the aggregation number N and dry volume V of $FC_{10}S$ for the contrast factor I_o, (b) the rod radius R for the form factor $P(Q)$, and (c) the aggregates' fractional ionization factor α for the structural factor $S(Q)$. To reduce free parameters in the fitting algorithm, we derive the rod length L from the constraint $N/L = 0.2$ obtained

TABLE 1: Parameters Used in the Model Fitting (Rodlike Form Factor and MSA Structural Factor) for the SANS and SAXS Data of $FC_{10}S$ Water Solutions

	C (%)	*R* (Å)	*L* (Å)	N	*V* (Å^3)	a	σ*(Å)
SANS	4	23.3 ± 0.5	170 ± 20	34 ± 4	2370 ± 50	0.048 ± 0.01	97
SANS	2	21.1 ± 0.5	155 ± 20	31 ± 4	2320 ± 50	0.037 ± 0.01	97
SANS	1	21.2 ± 0.7	160*	32*	2320 ± 50	0.023 ± 0.01	90
SANS	0.5	19.5 ± 0.9	160 ± 25	32 ± 5	2220 ± 100	0.022 ± 0.01	87
SAXS	4	21.1 ± 0.5	140	34	2120 ± 50	0.048	97
SAXS	2	17.9 ± 1.0	125	31	2310 ± 50	0.037	97
SAXS	1	23.2 ± 1.0	130	32	2180 ± 100	0.023	90

C: sample concentration; *R* and *L*: rod radius and length; *N*, *V*, and α: aggregation number, dry volume, and ionization constant for $FC_{10}S$; σ: effective diameter of the aggregates for the MSA model. *Denotes the fixed parameters during the fitting procedure. *N*, α, and σ are common parameters for SANS and SAXS data of the same concentration. The smearing effect of *I*(*Q*) due to the beam divergence and the wavelength dispersion of the beam were taken into account for the SANS and SAXS data, respectively, in the fitting algorithm.

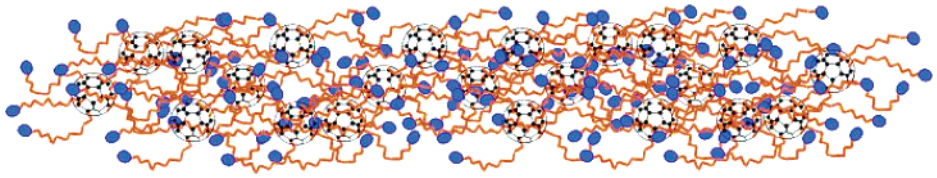

Figure 5. Proposed schematic view for $FC_{10}S$ aggregates.

previously from the model-independent approximation, and use the hydrodynamic radius R_h calculated from the rod length and radius for the effective hard-sphere radius $\sigma/2$ of the MSA model.[13] Then, we conjunctly fit the corresponding SANS and SANS data of the same concentration for sharing the common parameters *N*, σ, and α.[21] The fitting results are shown in Figure 3 and Figure 4 for the SANS and SAXS data, respectively. The structural parameters commonly determined by the SANS and SAXS data for the $FC_{10}S$ aggregates are summarized in Table 1. Note, we have taken into account the instrument resolution and neglected the sharp-rising low-*Q* data in the fitting procedure. Although, we can also fit the low-*Q* data with an additional term of $I_{add}(Q) \propto Q^{-4}$ in the fitting algorithm.

From the fitting result in Table 1, we conclude that the aggregation structure of $FC_{10}S$ is relatively insensitive to the concentration studied. In average, we have a dry volume $V = 2270 \pm 100$ Å^3, a mean aggregation number $N = 32 \pm 2$, and a rod radius $R = 21.3 \pm 1.6$ Å. The full length of the aggregation of $FC_{10}S$ determined from SANS is 162 ± 8 Å, with the C_{60} distributing mainly in a smaller region of 130 Å (from SAXS).

With the fitted structural parameters, we have constructed an aggregation model (Figure 5) that has a relatively homogeneous cross-section and arms that extend out (15 Å) from each side of the $FC_{10}S$ aggregates to reflect the different aggregation lengths observed by SANS and SAXS. Furthermore, the fractal ionization factor $\alpha \approx 0.032 \pm 0.012$, fitted from the MSA model with $\sigma = 93$ Å, corresponds to a surface charge $Z = 6\alpha N \approx 6$ for each aggregate of $FC_{10}S$ of six sulfobutoxypentyl arms. Although we have good-fitting results for the data of lower concentrations, our model fitting curves, however, deviate gradually from the data of higher concentrations. The situation does not improve much even when we use a core−shell rod structure in the model fitting.

We have also measured SAXS for $FC_{10}S$ water solutions with salt added for reducing the charge interaction peak.[14] With a much smaller charge interaction ($S(Q) \sim 1$), the rodlike structure, $R = 21 \pm 1$ Å, and $L = 150 \pm 10$ Å obtained for the $FC_{10}S$ aggregates in the saline solutions match closely with that given by the model fitting previously. With the much-reduced structure factor *S*(*Q*) (or charge interactions), we have also observed that the aggregates grow continuously in length with a nearly constant radius as temperature increases, in our previous study.[14] The lack of an energy barrier in growing the length of the rodlike $FC_{10}S$ aggregates implies that the aggregates have a polydispersity in the longitudinal direction, while keeping the radius relatively constant. In fact, the increasingly larger polydispersity in solutions of higher $FC_{10}S$ concentrations may account for the increasingly larger discrepancy between our model fitting and the SAS data.

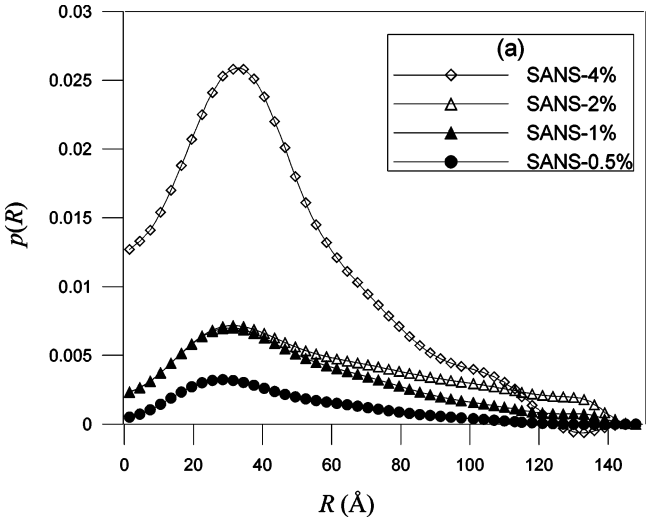

Figure 6. Pair distance distribution functions *p*(*r*) obtained for the corresponding SANS data at different concentrations.

Alternatively, from the generalized indirect Fourier transformation (GIFT),[22,23] a model-independent method for a pair distance distribution function *p*(*r*), we also obtain a rodlike *p*(*r*) (Figure 6) of similar radius and length for $FC_{10}S$ aggregates as that determined from the model fitting.

5. Conclusions and Discussion

We have obtained detailed aggregation characteristics of $FC_{10}S$ in water solutions using SANS and SAXS. Compared to the short-arm fullerene-based ionomer FC_4S of a globular aggregation shape,[24] the long-arm fullerene-based ionomers $FC_{10}S$ have a considerably different aggregation behavior, including the aggregation shape, size, and charge interaction characteristics. Table 2 summarizes the influences of arm length on the aggregation characteristics of these two fullerene-based

TABLE 2: Comparison of the Aggregation Characteristics of $FC_{10}S$ and FC_4S (data from previous study[24])

	N	N/L (Å^{-1})	R_g (Å)	a	shape
$FC_{10}S$	32	0.2	50	0.03	rodlike
FC_4S	5	0.07	20	0.15	globular

N: Aggregation number. N/L: Aggregation number per unit length. R_g: Radius of gyration. For rodlike particles,[8] $R_g = (R^2/2+L^2/12)^{1/2}$.α: Fractional ionization constant for the aggregates.

ionomers, $FC_{10}S$ and FC_4S. Specifically, $FC_{10}S$ aggregates have a similar cross-section as that for FC_4S aggregates, but a significant longer aggregation length and a much higher linear packing density N/L of 0.2. From the structural parameters obtained, $FC_{10}S$ aggregates, most likely, have the long sulfobutoxypentyl arms bending along the rod-axis of the aggregates. In such folding, arm length becomes important in the growth of the aggregate, since longer arms can provide better mutual penetrations for a better hydrophobic environment. Also, the mutual penetration of the arms helps the SO_3Na headgroups of the sulfobutoxypentyl arms reaching out more toward the C_{60} cages of neighboring $FC_{10}S$ for better charge mediation. This may explain the much smaller ionization factor of 0.03 observed for the $FC_{10}S$ aggregates of longer sulfobutoxypentyl arms, compared to the 0.15 for the FC_4S aggregates of shorter sulfobutyl arms.[24]

Acknowledgment. We acknowledge the support of the NIST for the SANS beam time. This work was supported by the grant for the user-training program of the TRR2 project of the Institute of Nuclear Energy Research and the National Science Council, grant NSC91-2113-M-007-037(T.-L. Lin).

References and Notes

(1) Wang, I.-C.; Tai, L. A.; Lee, D. D.; Kanakamma, P. P.; Shen, C. K.-F.; Luh, T.-Y.; Cheng, C. H.; Hwang, K. C. *J. Med. Chem.* **1999**, *42*, 4614.

(2) Lai, Y. L.; Chiou, W.-Y.; Lu, F. J.; Chiang, L. Y. *Brit. J. Pharmacol.* **1999**, *126*, 778.

(3) Huang, S. S.; Chen, Y. H.; Chiang, L. Y.; Tsai, M. C. *Fullerene Sci. Technol.* **1999**, *7* (4), 551.

(4) Jeng, U.; Lin, T.-L.; Chang, T.-S.; Lee, H.-Y.; Hsu, C.-H.; Hseih, Y.-W.; Canteenwala, T.; Chiang, L. Y. *Prog. Colloid. Polym. Sci.* **2001**, *118*, 232−237.

(5) Penfold, J.; Staples, E.; Tucker, I. *Adv. Colloid Interface Sci.* **1996**, *68*, 31.

(6) Purcell, I. P.; Lu, J. R.; Thomas, R. K.; Howe, A. M.; Penfold, J. *Langmuir* **1998**, *14*, 1637.

(7) Lin, T.-L. *Physica B* **1992**, *180&181*, 505.

(8) Feigin, L. A.; Svergun, D. I. *Structure Analysis by Small-Angle X-ray and Neutron Scattering*; Plenum: New York, 1987; p69.

(9) Chen, S. H. *Annu. Rev. Phys. Chem.* **1986**, *37*, 351.

(10) Porod, G. *Small-Angle X-ray Scattering*; Glatter, O., Kratky, O., Eds.; Academic Press: London, 1982; Chapter 2, p32.

(11) Chen, S. H.; Lin, T. L. *Methods of Experimental Physics − Neutron Scattering in Condensed Matter Research*; Sköld, K., Price, D. L., Eds.; Academic Press: New York, 1987; Vol. 23B, Chapter 16.

(12) Hayter, J.; Penfold, J. *Mol. Phys.* **1981**, *42*, 109.

(13) Schmitz, K. S. *An Introduction to Dynamic Light Scattering by Macromolecules*; Academic Press: New York, 1980; p56.

(14) Liu, W.-J.; Jeng, U.; Lin, T.-L.; Canteenwala, T.; Chiang, L. Y. *Fullerene Sci. Technol.* **2001**, *9*, 131.

(15) Glinka, C. J.; Barker, J. G.; Hammouda, B.; Krueger, S.; Moyer, J. J.; Orts, W. J. *J. Appl. Crystallogr.* **1998**, *31*, 430.

(16) Linliu, K.; Chen, S.-A.; Yu, T. L.; Lin, T.-L.; Lee, C.-H.; Kai, J.-J.; Chang, S.-L.; Lin, J. S. *J. Polym. Res.* **1995**, *2*, 63.

(17) Lin, T.-L.; Chen, S.-H.; Gabriel, N. E.; Roberts, M. F. *J. Phys. Chem.* **1987**, *91*, 406.

(18) Guinier, A.; Fournet, G. *Small-Angle Scattering of X-rays*; John Wiley and Sons: New York, 1955.

(19) Glatter, O.; Kratky, O. *Small Angel X-ray Scattering*; Academic Press Inc., London, New York, 1980.

(20) Sheu, E. Y.; Wu, C.-F.; Chen, S.-H. *J. Phys. Chem.* **1986**, *90*, 4179.

(21) Brunner-Popela, J.; Glatter, O. *J. Appl. Crystallogr.* **1997**, *30*, 431.

(22) Fritz, G.; Bergmann, A.; Glatter, O. *J. Chem. Phys.* **2000**, *113*, 9733.

(23) Cabane, B.; Duplessix, R.; Zemb, T. *J. Physique* **1985**, *46*, 2161.

(24) Jeng, U.; Lin, T.-L.; Hu, Y.; Chang, T.-S.; Canteenwala, T.; Chiang, L. Y.; Frielinghausc, H. *J. Phys. Chem. B*, *J. Phys. Chem. A* **2002**, *106*, 12209.